Yue Qi, Chris J. Hawkesworth, Qiang Wang, Derek A. Wyman, Zheng-Xiang Li, Han Dong, Tao Ma, Fukun Chen, Wan-Long Hu, and Xiu-Zheng Zhang, 2020, Syn-collisional magmatic record of Indian steep subduction by 50 Ma: GSA Bulletin, https://doi.org/10.1130/B35498.1.

Supplemental Material

Text S1. Analytical methods including Zircon U-Pb dating and Hf isotope and whole rock geochemistry.

Figure S1. The 1:5000 scale geological cross-section from A to A'. Cross section locations are shown on the Fig. 1B.

Figure S2. SiO_2 and major and trace element diagrams of the Lopu Range batholith.

Figure S3. Large scale evolution if the continental collision and subduction.

Table S1. Zircon U-Pb isotopic data of the Lopu Range batholith.

Table S2. Major (wt%) and trace (ppm) elementcontentsof the Lopu Range batholith.

Text S2. References cited in Data 1 and 3.

Data 1. Zircon Hf isotopic ratios of Lopu Range batholith and igneous rocks.

Data 2. Samples in Fig. 5B.

Data 3. Sr and Nd isotopic composition of the Lopu Range batholith.

[1] Text S1 **Analytical methods**

ZIRCON U-Pb DATING AND HF ISOTOPE

Zircons were separated from fresh samples using conventional heavy liquid and magnetic techniques and then hand-picked under a binocular microscope. Zircon grains were casted in the epoxy mount and polished to about half their thickness for analysis. Cathodoluminescence (CL) images of zircons were conducted at the State Key Laboratory of Isotope Geochemistry, Guangzhou Institute of Geochemistry, Chinese Academy of Sciences (SKLaBIG GIG CAS).

Zircon U-Pb dating was performed using LA-ICP-MS at the Institute of Geology and Geophysics, Chinese Academy of Sciences. Laser ablation was accomplished using a Geolas-193 laser-ablation system equipped with a 193 nm ArFexcimer laser and connected to an ELAN6100 DRC ICP-MS. The analyses were conducted with a spot diameter of 44 μm with a typical ablation time of ~30 s for 200 cycles of each measurement, an 8 Hz repetition rate, and a laser power of 100mJ/pulse. A more detailed description of the analytical technique is provided by Xie et al. (2008).

Secondary ion mass spectrometry (SIMS) zircon U-Pb analyses were conducted using a CAMECAIMS-1280-HR system at the SKLaBIG GIG CAS. Analytical procedures is similar to that described by Li et al. (2009). The O_2^- primary ion beam with an intensity of ~10 nA was accelerated at −13kV. The ellipsoidal spot is ~20 μm × 30 μm in size. The aperture illumination mode (Kohler illumination) was used with a 200 μm primary beam mass filter (PBMF) aperture to produce even sputtering over the entire analyzed area. Oxygen flooding was used to increase the O^2 pressure to 5×10^{-6} Torr in the sample chamber, enhancing Pb+ sensitivity to a value of ~25cps/nA/ppm for zircon. This great enhancement of Pb+ sensitivity is crucial to improve precision of $^{207}Pb/^{206}Pb$ zircon measurement. Positive secondary ions were extracted with a 10 kV potential. In the secondary ion beam optics, a 60 ± 5eV energy window was used, together with a mass resolution of ~5400. Rectangular lenses were activated in the secondary ion optics to increase the transmission at high mass resolution. A single electron multiplier was used in ion-counting mode to measure secondary ion beam intensities by the peak jumping sequence: 196 ($^{90}Zr_2{}^{16}O$, matrix reference), 200 ($^{92}Zr_2{}^{16}O$), 200.5 (background), 203.81 ($^{94}Zr_2{}^{16}O$, for mass calibration), 203.97 (Pb), 206 (Pb), 207 (Pb), 208 (Pb), 209 ($^{177}Hf^{16}O_2$), 238 (U), 248 ($^{232}Th^{16}O$), 270 ($^{238}U^{16}O_2$), and 270.1 (reference mass). The integration time, for these mass are 1.04, 0.56, 4.16, 0.56, 6.24, 4.16, 6.24, 2.08, 1.04, 2.08, 2.08, 2.08, and 0.24 s, respectively. Each measurement consisted of seven cycles, and the total analytical time per measurement was ~12 min.

Calibration of Pb/U ratios is relative to the standard zircon Plesovice (337.13 Ma, Sláma et al., 2008), which was analyzed once every four unknowns, based on an observed linear relationship between ln ($^{206}Pb/^{238}U$) and ln ($^{238}U^{16}O_2/^{238}U$) (Whitehouse et al., 1997). A long-term uncertainty of 1.5% (1RSD) for $^{206}Pb/^{238}U$ measurements of the standard zircons was propagated to the unknowns (Li et al., 2010), despite that the measured $^{206}Pb/^{238}U$ error in a specific session is generally around 1% (1 RSD) or less. U and Th concentrations of unknowns were also calibrated relative to the standard zircon Plesovice, with Th and U concentrations of 78 and 755 ppm, respectively (Sláma et al., 2008). Measured compositions were corrected for common Pb using non-radiogenic ^{204}Pb. A secondary standard zircon Qinghu (Li et al., 2013) were analyzed as unknown to monitor the relaiblity of the whole procedure. Uncertainties on single analyses are reported at the 1σ level; mean ages for pooled U-Pb analyses are quoted with a 95% confidence interval. Data reduction was carried out using the Isoplot/Ex 3 software (Ludwig, 2003).

In situ zircon Hf isotope measurements were subsequently carried out on U-Pb dated zircons using LA-MC-ICP-MS with a beam size of 60 μm and laser pulse frequency of 8 Hz at the MC-ICPMS laboratory of SKLIG GIG CAS. Details of instrumental conditions and data acquisition were given in Wu et al., (2006).

WHOLE ROCK GEOCHEMISTRY

Major element oxides of whole rock samples were determined in the Hubei Province Geological Experimental Testing Center. The accuracy of the XRF analyses is between 1 and 5%. Trace elements were analyzed by inductively coupled plasma mass spectrometry (ICP-MS), using a Perkin-Elmer Sciex ELAN 6000 instrument at SKLaBIG GIG CAS. Analytical procedures are the same as those described by Li et al., (2002). Repeated runs give 3% RSD (relative standard deviation) for most elements of reference materials analyzed by ICP-MS.

Separation and purification of the Sr-Nd isotope were performed at the Key Laboratory of Crust-Mantle Materials and Environments, University of Science and Technology of China (USTC), Hefei. The digested samples were evaporated at 130 °C, and subsequently evaporated at 150 °C and redissolved in 6 N HCl twice to remove fluorides. In a final step, the samples were redissolved in 1 ml of 3N HCl and centrifuged. Sr and rare-earth elements were isolated on quartz columns by conventional ion exchange chromatography with a 5 ml resin bed of Bio Rad AG 50W-X12, 200–400 mesh. Nd was separated from rare-earth elements on quartz columns using 1.7 ml Teflon powder coated with HDEHP, di(2-ethylhexyl)orthophosphoric acid, as cation exchange medium. A more detailed description is provided by Chen et al. (2000).

Sr and Nd isotopic ratios of selected samples were determined using a Micromass Isoprobe multi-collector mass spectrometer (MC-ICP-MS) at SKLaBIG GIG-CAS. Analytical procedures are similar to those described in Li et al., (2004). Measured ^{87}Sr/^{86}Sr and ^{143}Nd/^{144}Nd ratios were normalized to ^{86}Sr/^{88}Sr = 0.1194 and ^{146}Nd/^{144}Nd = 0.7219, respectively. Analyses of NBS-SRM 987 and the Shin Etsu JNdi-1 standards during this study yielded an average values of ^{87}Sr/^{86}Sr = 0.710253 ± 10 (n = 10) and ^{143}Nd/^{144}Nd = 0.512109 ± 3 (n = 6).

REFERENCES CITED

Chen, F., Hegner, E., and Todt, W., 2000, Zircon ages and Nd isotopic and chemical compositions of orthogneisses from the Black Forest, Germany: evidence for a Cambrian magmatic arc: International Journal of Earth Sciences, v. 88, p. 791–802, https://doi.org/10.1007/s005310050306.

Li, X.H., Liu, Y., Li, Q.L., Guo, C.H., and Chamberlain, K.R., 2009, Precise determination of Phanerozoic zircon Pb/Pb age by multicollector SIMS without external standardization: Geochemistry Geophysics Geosystems, v. 10, Q04010.

Li, X.H., Long, W.G., Li, Q.L., Liu, Y., Zheng, Y.F., Yang, Y.H., Chamberlain, K.R., Wan, D.F., Guo, C.H., Wang, X.C., and Tao, H., 2010, Penglai Zircon Megacrysts: A Potential New Working Reference Material for Microbeam Determination of Hf–O Isotopes and U-Pb Age: Geostandards and Geoanalytical Research, v. 34, p. 117–134, https://doi.org/10.1111/j.1751-908X.2010.00036.x.

Li, X., Tang, G., Gong, B., Yang, Y., Hou, K., Hu, Z., Li, Q., Liu, Y., and Li, W., 2013, Qinghu zircon: A working reference for microbeam analysis of U-Pb age and Hf and O isotopes: Chinese Science Bulletin, v. 58, p. 4647–4654, https://doi.org/10.1007/s11434-013-5932-x.

Li, X.H., Liu, D.Y., Sun, M., Li, W.X., Liang, X.R., and Liu, Y., 2004, Precise Sm-Nd and U-Pb isotopic dating of the supergiant Shizhuyuan polymetallic deposit and its host granite, SE China: Geological Magazine, v. 141, p. 225–231, https://doi.org/10.1017/S0016756803008823.

Li, X.H., Zhou, H.W., Chung, S.L., Lo, C.H., Wei, G.J., Liu, Y., and Lee, C.Y., 2002, Geochemical and Sr-Nd isotopic characteristics of late paleogene ultrapotassic magmatism in southeastern Tibet: International Geology Review, v. 44, p. 559–574, https://doi.org/10.2747/0020-6814.44.6.559.

Ludwig, K.R., 2003, User's Manual for Isoplot 3.00: A Geochronological Toolkit for Microsoft Excel: Berkeley California.

Sláma, J., Košler, J., Condon, D.J., Crowley, J.L., Gerdes, A., Hanchar, J.M., Horstwood, M.S.A., Morris, G.A., Nasdala, L., Norberg, N., Schaltegger, U., Schoene, B., Tubrett, M.N., and Whitehouse, M.J., 2008, Plešovice zircon — A new natural reference material for U-Pb and Hf isotopic microanalysis: Chemical Geology, v. 249, p. 1–35, https://doi.org/10.1016/j.chemgeo.2007.11.005.

Whitehouse, M.J., Claesson, S., Sunde, T., and Vestin, J., 1997, Ion microprobe U-Pb zircon geochronology and correlation of Archaean gneisses from the Lewisian Complex of Gruinard Bay, northwestern Scotland: Geochimica et Cosmochimica Acta, v. 61, p. 4429–4438, https://doi.org/10.1016/S0016-7037(97)00251-2.

Wu, F.Y., Yang, Y.H., Xie, L.W., Yang, J.H., and Xu, P., 2006, Hf isotopic compositions of the standard zircons and baddeleyites used in U-Pb geochronology: Chemical Geology, v. 234, p. 105–126, https://doi.org/10.1016/j.chemgeo.2006.05.003.

Xie, L.W., Zhang, Y.B., Zhang, H.H., Sun, J.F., and Wu, F.Y., 2008, In situ simultaneous determination of trace elements, U-Pb and Lu-Hf isotopes in zircon and baddeleyite: Chinese Science Bulletin, v. 53, p. 1565–1573.

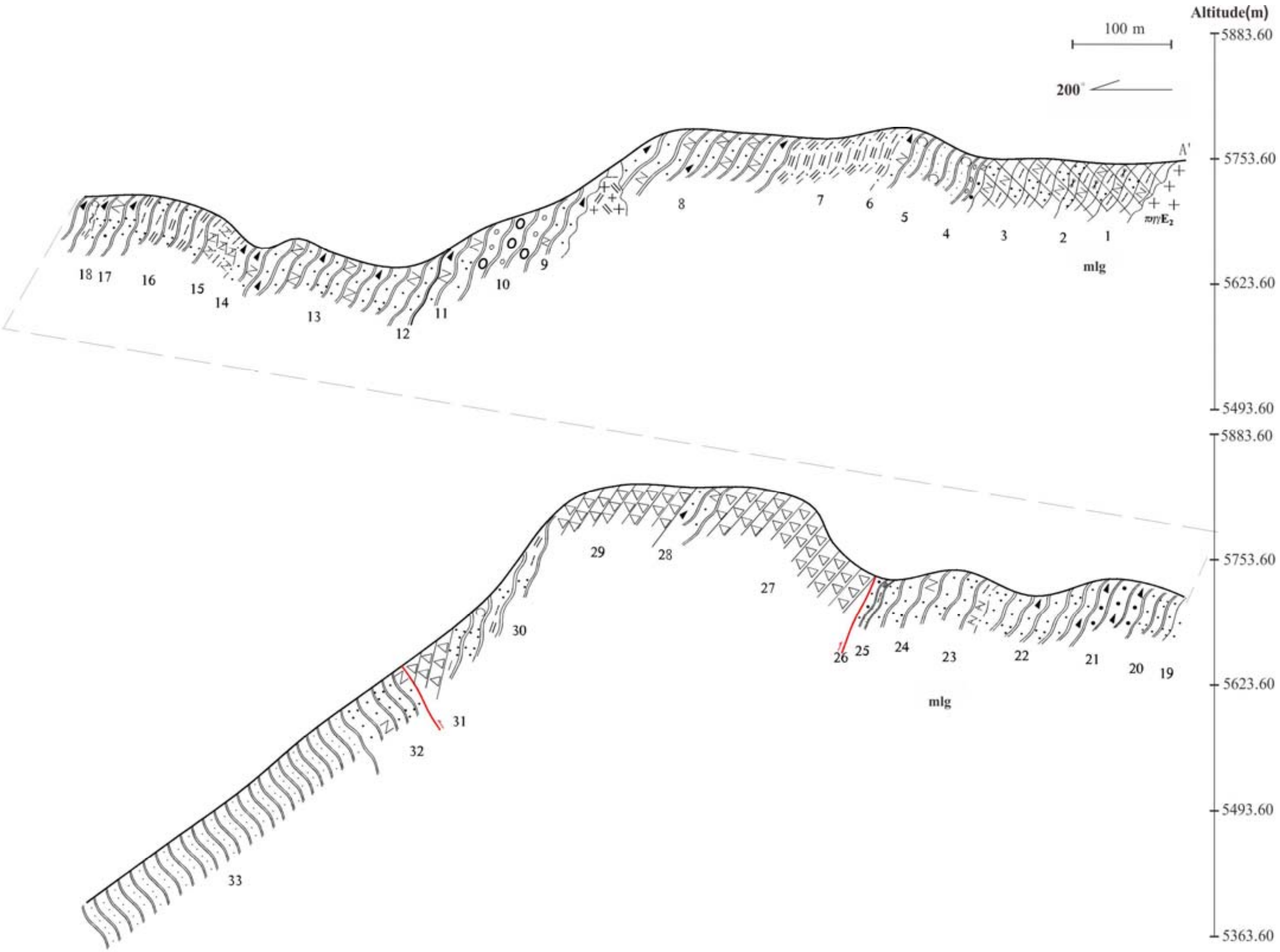

Altitude(m)
100 m
200°
A'
5883.60
5753.60
5623.60
5493.60
5883.60
5753.60
5623.60
5493.60
5363.60
mlg
mlg
1 2 3 4 5 6 7 8 9 10 11 12 13 14 15 16 17 18
19 20 21 22 23 24 25 26 27 28 29 30 31 32 33

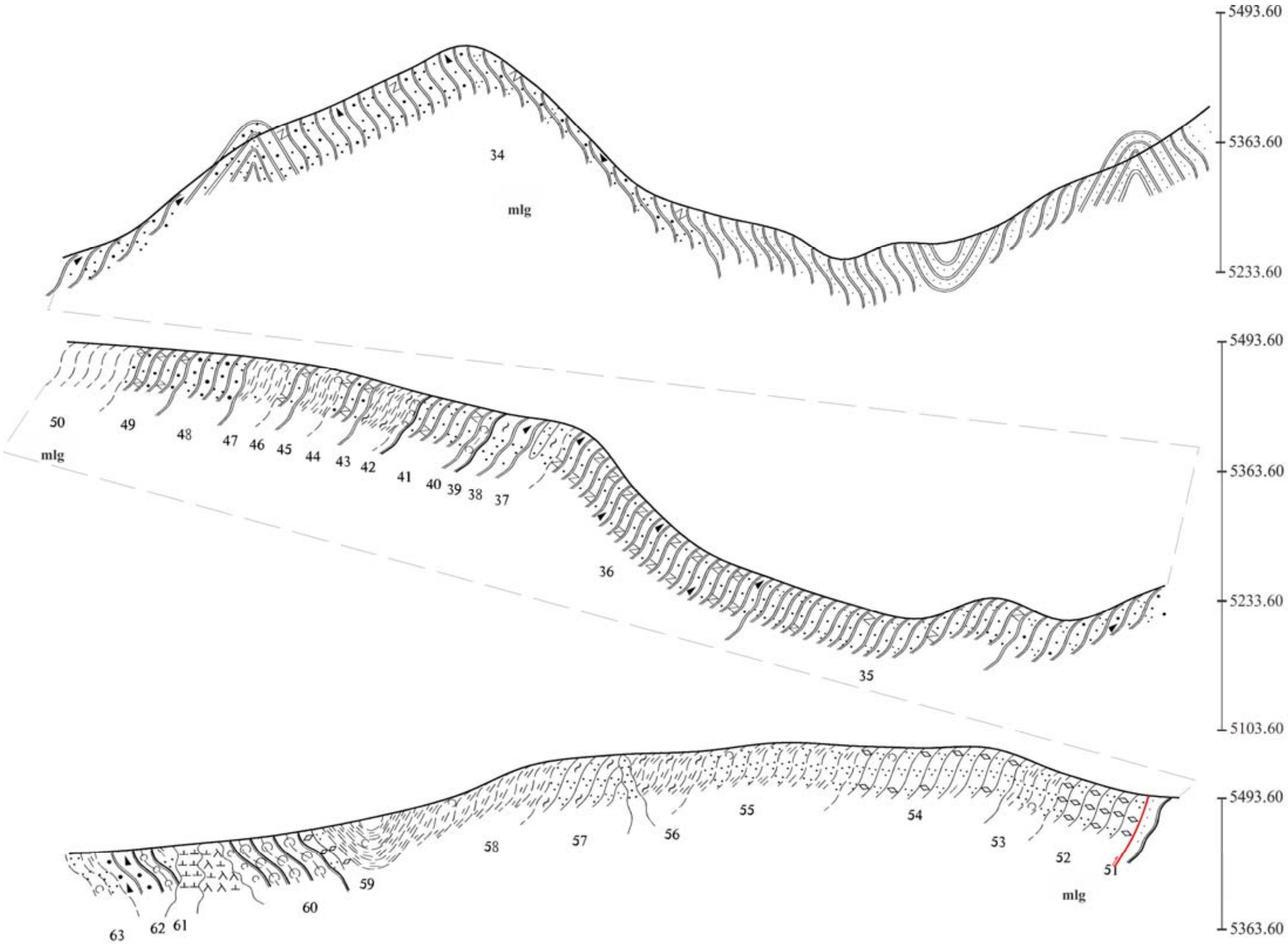
5493.60
5363.60
5233.60
34
mlg
5493.60
5363.60
5233.60
5103.60
50 49 48 47 46 45 44 43 42 41 40 39 38 37
mlg
36
35
5493.60
5363.60
55 54 53 52 51
58 57 56
59 60
63 62 61
mlg

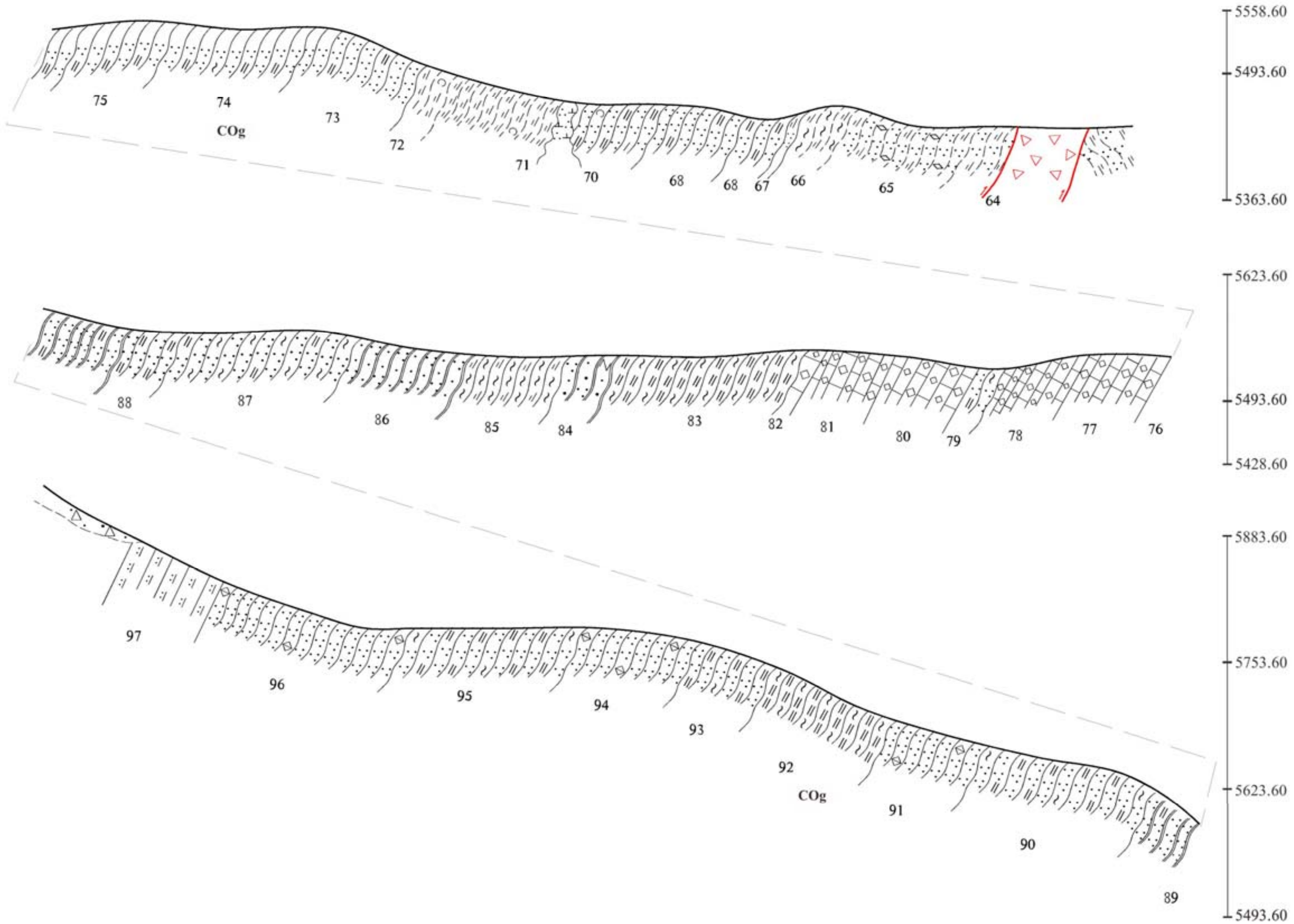

5558.60
5493.60
5363.60
75
74
73
COg
72
71
70
68
68
67
66
65
64
5623.60
5493.60
5428.60
88
87
86
85
84
83
82
81
80
79
78
77
76
5883.60
5753.60
5623.60
5493.60
97
96
95
94
93
92
COg
91
90
89

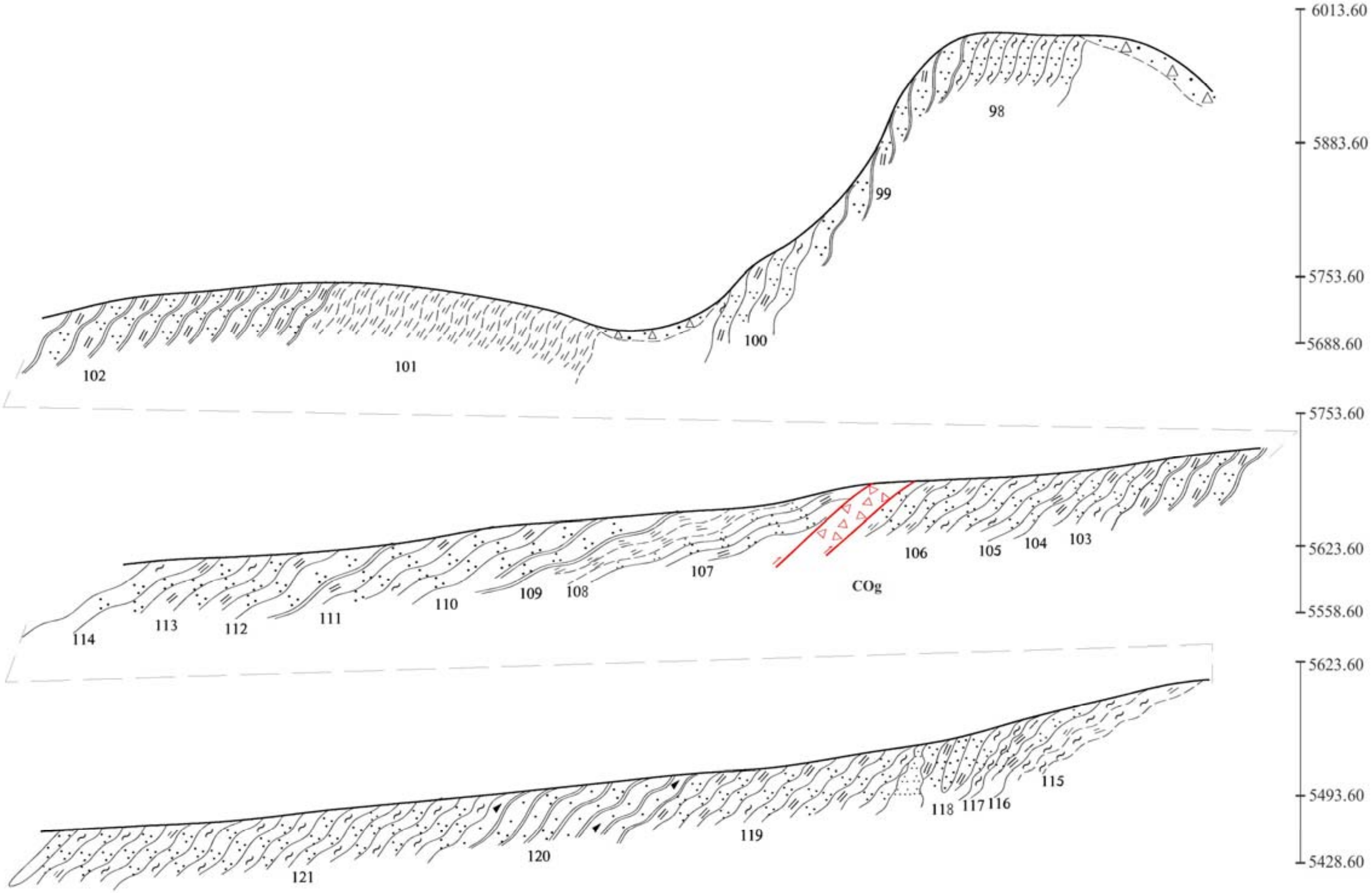

6013.60
5883.60
5753.60
5688.60
98
99
100
101
102
5753.60
5623.60
5558.60
103
104
105
106
COg
107
108
109
110
111
112
113
114
5623.60
5493.60
5428.60
115
116
117
118
119
120
121

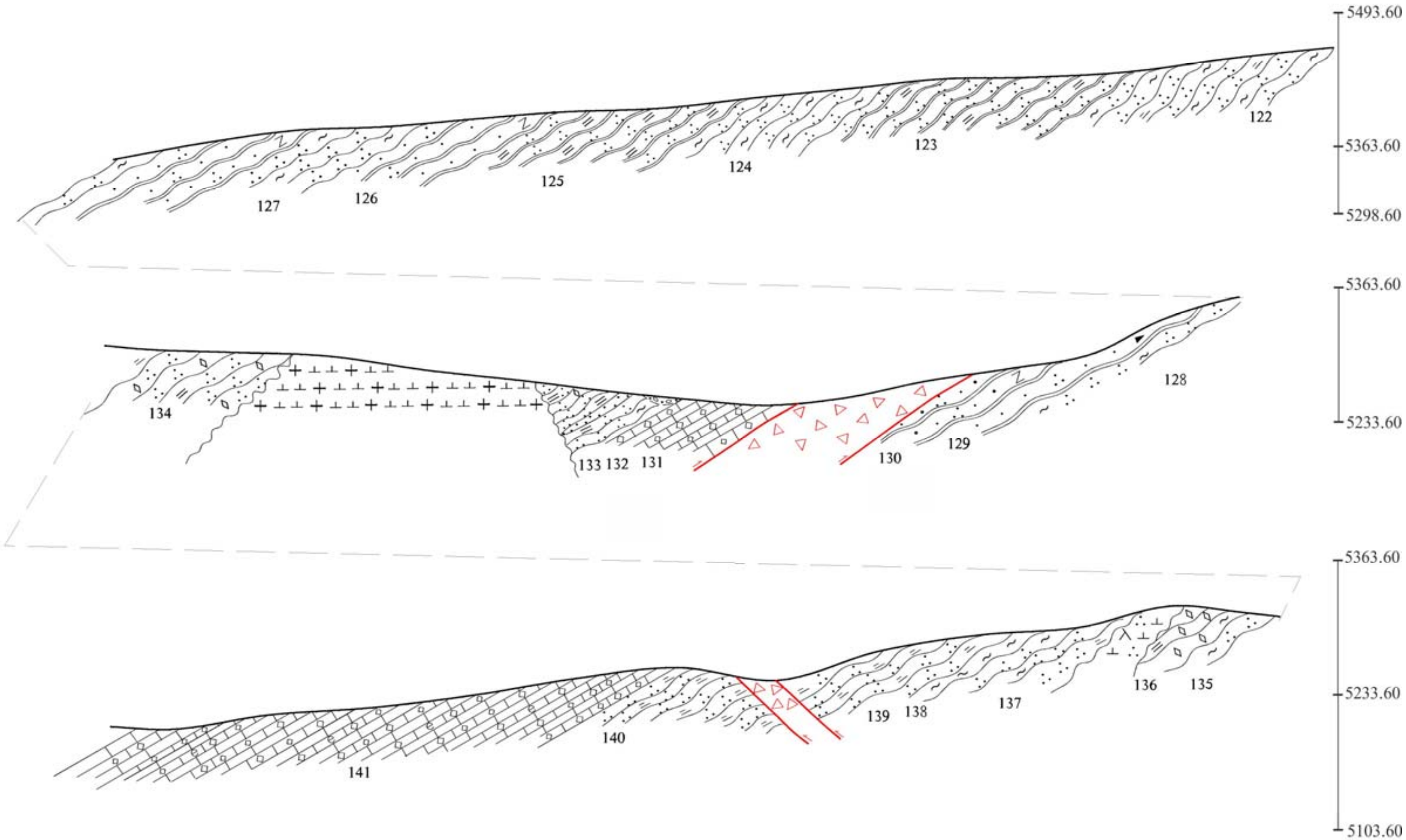

5493.60
5363.60
5298.60
122
123
124
125
126
127
5363.60
5233.60
128
129
130
131
132
133
134
5363.60
5233.60
5103.60
135
136
137
138
139
140
141

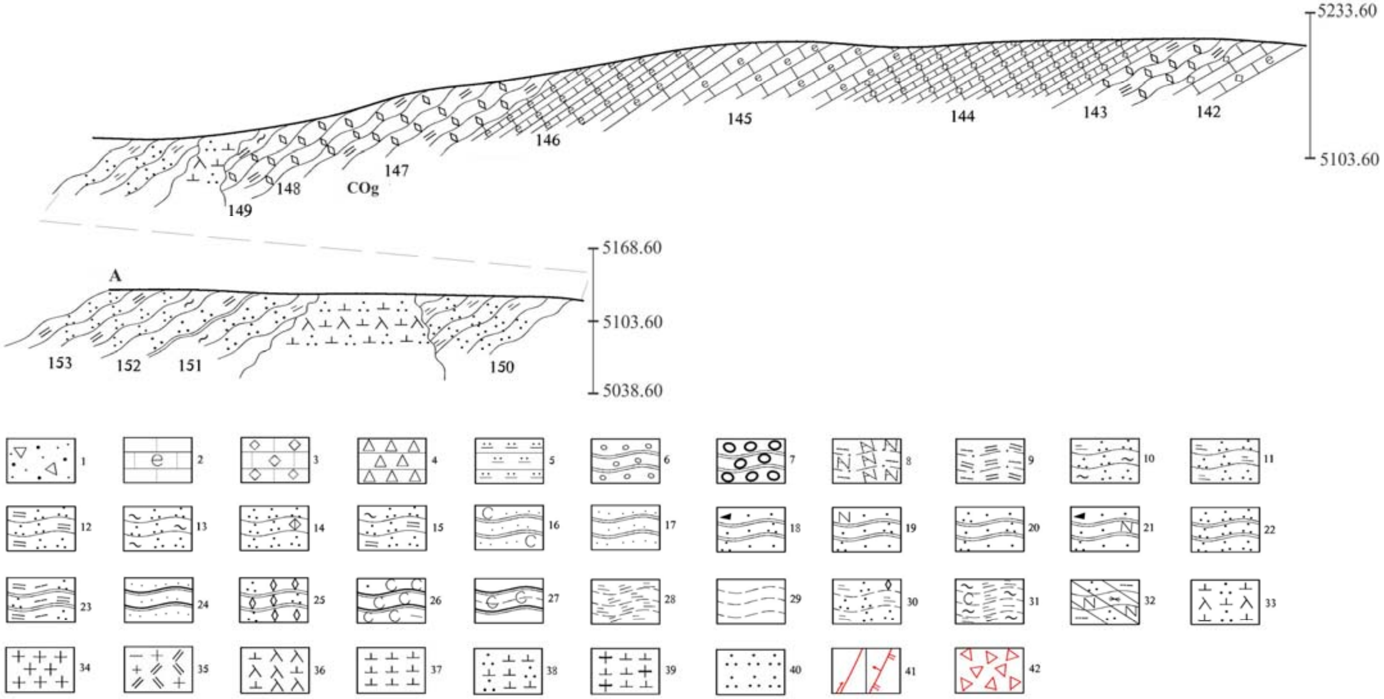
5233.60
5103.60
146
145
144
143
142
147
148
COg
149
5168.60
A
5103.60
5038.60
153
152
151
150
1 2 3 4 5 6 7 8 9 10 11
12 13 14 15 16 17 18 19 20 21 22
23 24 25 26 27 28 29 30 31 32 33
34 35 36 37 38 39 40 41 42

Figure S1. The 1:5000 scale geological cross-section from A to A'. Cross section locations are shown on the Fig. 1b. 1 to 153 is the layer number. Legend: 1: moraine deposit, 2: bioclastic limestone, 3: limestone, 4: volcanic breccia, 5: silicalite, 6: fine-metaconglomerate, 7: coarse-metaconglomerate, 8: biotite plagioclase leptynite, 9: biotite monzo-leptynite, 10: sericite-chlorite-quartz schist, 11: sericite-quartz schist, 12: muscovite-quartz schists, 13: chlorite-quartz schist, 14: quartz schist, 15: chlorite-muscovite-quartz schist, 16: carbon meta-siltstone, 17: meta-siltstone, 18: meta-debris quartz sandstone, 19: meta-feldspar quartz sandstone, 20: meta-quartz sandstone, 21: meta-debris feldspar quartz sandstone, 22: quartzite, 23: two-mica quartzite, 24: aleuropelitic slate, 25: quartz-calcite, 26: argillaceous slate, 27: carbonaceous slate, 28: sericite-phyllite, 29: phyllite, 30: quartz-calcite-sericite-phyllite, 31: chlorite-sericite-phyllite, 32: actinolite-biotite hornstone, 33: quartz-diorite porphyry, 34: granite, 35: biotite monzonite, 36: diorite-porphyrite, 37: diorite, 38: quartz diorite, 39: granodiorite-porphyry, 40: quartz vein, 41: thrust fault, 42: fault breccia.

Figure S2 SiO_2 and major and trace element diagrams of the Lopu Range batholith

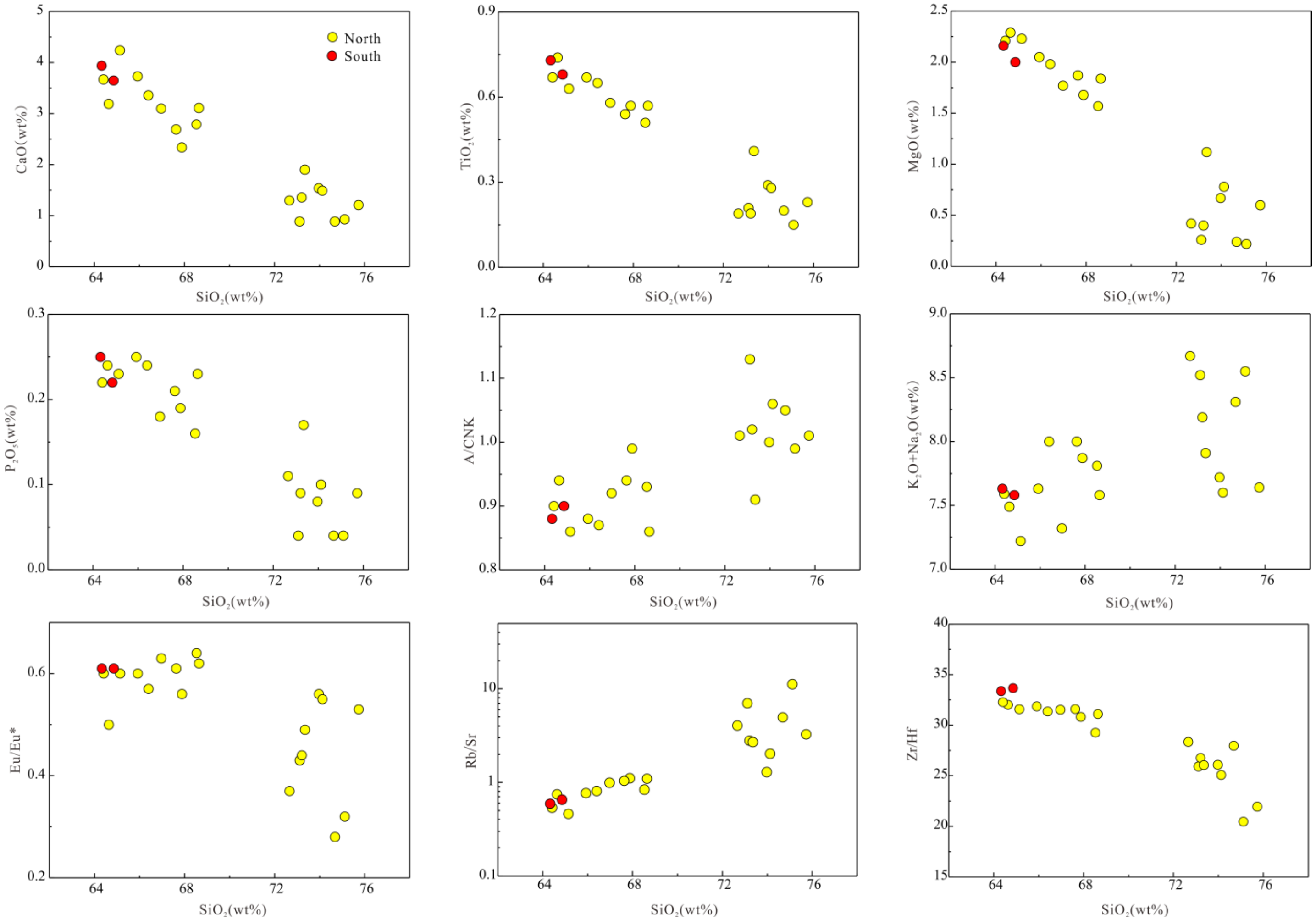

Table S1 Zircon U-Pb isotopic data of the Lopu Range batholith

Sample spots	Th ppm	U ppm	Pb* ppm	Th/U	Ratios $^{207}Pb/^{206}Pb$	1σ	$^{207}Pb/^{235}U$	1σ	$^{206}Pb/^{238}U$	1σ	Age(Ma,1σ) $^{207}Pb/^{206}Pb$	1σ	$^{207}Pb/^{235}U$	1σ	$^{206}Pb/^{238}U$	1σ
LA-ICP-MS																
North																
PM4-5 (29°58'52.2" 84°59'25.4")																
PM4-5-01	365	530	5	0.69	0.06080	0.00263	0.06424	0.00264	0.00766	0.00018	632	91	63.2	2.5	49.2	1.1
PM4-5-02	997	980	9	1.02	0.04730	0.00213	0.04934	0.00214	0.00757	0.00017	64	105	48.9	2.1	48.6	1.1
PM4-5-03	1998	1377	15	1.45	0.05719	0.00176	0.05997	0.00176	0.00761	0.00016	498	67	59.1	1.7	48.8	1.0
PM4-5-04	608	1146	10	0.53	0.05347	0.00242	0.05609	0.00243	0.00761	0.00018	349	99	55.4	2.3	48.9	1.1
PM4-5-05	573	562	5	1.02	0.04139	0.00316	0.04466	0.00331	0.00782	0.00021	0	0	44.4	3.2	50.2	1.3
PM4-5-06	867	1730	15	0.50	0.05362	0.00221	0.05829	0.00229	0.00788	0.00018	355	90	57.5	2.2	50.6	1.1
PM4-5-07	431	322	3	1.34	0.04718	0.00557	0.05035	0.00578	0.00774	0.00026	58	260	49.9	5.6	49.7	1.7
PM4-5-08	479	495	5	0.97	0.04696	0.00406	0.05128	0.00428	0.00792	0.00023	47	195	50.8	4.1	50.8	1.5
PM4-5-09	702	582	6	1.21	0.04711	0.00374	0.04941	0.00379	0.00761	0.00021	54	180	49	3.7	48.8	1.4
PM4-5-10	403	591	6	0.68	0.05876	0.00362	0.06520	0.00385	0.00805	0.00021	558	129	64.1	3.7	51.7	1.4
PM4-5-11	279	643	5	0.43	0.04641	0.00345	0.04872	0.00352	0.00761	0.00020	19	169	48.3	3.4	48.9	1.3
PM4-5-12	466	729	7	0.64	0.04857	0.00313	0.05185	0.00321	0.00774	0.00020	127	145	51.3	3.1	49.7	1.3
PM4-5-13	741	948	9	0.78	0.04902	0.00481	0.05329	0.00500	0.00788	0.00027	149	215	52.7	4.8	50.6	1.7
PM4-5-14	399	404	4	0.99	0.04462	0.00385	0.04728	0.00395	0.00768	0.00022	0	122	46.9	3.8	49.3	1.4
PM4-5-15	494	850	7	0.58	0.05223	0.00304	0.05600	0.00312	0.00778	0.00020	296	127	55.3	3.0	49.9	1.3
PM4-5-16	532	757	6	0.70	0.04599	0.00340	0.04865	0.00347	0.00767	0.00021	0	166	48.2	3.4	49.3	1.3
PM4-5-17	665	644	6	1.03	0.04839	0.00344	0.05241	0.00359	0.00785	0.00021	118	160	51.9	3.5	50.4	1.4
PM2-63 (29°58'1" 84°39'27.7")																
PM2-63-01	405	421	4	0.96	0.04697	0.00429	0.05032	0.00447	0.00777	0.00018	48	205	49.9	4.3	49.9	1.2
PM2-63-02	392	418	4	0.94	0.04290	0.00451	0.04599	0.00472	0.00777	0.00020	0	69	45.7	4.6	49.9	1.3
PM2-63-03	272	286	3	0.95	0.04663	0.00489	0.05147	0.00526	0.00800	0.00021	30	234	51	5.1	51.4	1.3

Table S1 (Continued)

Sample spots	Th ppm	U ppm	Pb* ppm	Th/U	Ratios $^{207}Pb/^{206}Pb$	1σ	$^{207}Pb/^{235}U$	1σ	$^{206}Pb/^{238}U$	1σ	Age(Ma,1σ) $^{207}Pb/^{206}Pb$	1σ	$^{207}Pb/^{235}U$	1σ	$^{206}Pb/^{238}U$	1σ
PM2-63-04	1024	807	8	1.27	0.04823	0.00278	0.05111	0.00284	0.00768	0.00014	110	131	50.6	2.7	49.3	0.9
PM2-63-05	493	458	5	1.08	0.04934	0.00412	0.05320	0.00427	0.00782	0.00020	164	184	52.6	4.1	50.2	1.3
PM2-63-06	169	652	5	0.26	0.05001	0.00305	0.05320	0.00312	0.00771	0.00015	196	136	52.6	3.0	49.5	1.0
PM2-63-07	446	459	5	0.97	0.05274	0.00375	0.05561	0.00380	0.00765	0.00017	318	153	55	3.7	49.1	1.1
PM2-63-08	734	1642	14	0.45	0.04930	0.00194	0.05335	0.00202	0.00785	0.00012	162	90	52.8	1.9	50.4	0.7
PM2-63-09	416	500	5	0.83	0.04712	0.00367	0.05131	0.00387	0.00790	0.00017	55	176	50.8	3.7	50.7	1.1
PM2-63-10	484	451	4	1.07	0.04366	0.00389	0.04665	0.00404	0.00775	0.00018	0	76	46.3	3.9	49.8	1.1
PM2-63-11	399	406	4	0.98	0.04950	0.00436	0.05357	0.00459	0.00785	0.00018	172	194	53	4.4	50.4	1.2
PM2-63-12	318	629	6	0.51	0.04590	0.00291	0.05084	0.00311	0.00803	0.00016	0	139	50.4	3.0	51.6	1.0
PM2-63-13	290	456	4	0.64	0.04646	0.00353	0.05216	0.00384	0.00814	0.00017	21	173	51.6	3.7	52.3	1.1
PM2-63-14	373	448	4	0.83	0.05669	0.00410	0.06213	0.00431	0.00795	0.00018	479	153	61.2	4.1	51	1.2
PM2-63-15	192	213	2	0.90	0.04411	0.00634	0.04766	0.00671	0.00784	0.00025	0	215	47.3	6.5	50.3	1.6
PM3-40 (29°58'1.6" 84°47'43.9")																
PM3-40-01	1844	1281	15	1.44	0.04710	0.00195	0.04661	0.00186	0.00718	0.00010	54	97	46.3	1.8	46.1	0.7
PM3-40-02	1217	586	7	2.08	0.05049	0.00352	0.04993	0.00336	0.00717	0.00015	218	154	49.5	3.3	46.1	1.0
PM3-40-03	681	2856	22	0.24	0.04604	0.00140	0.04652	0.00135	0.00733	0.00009	0	71	46.2	1.3	47.1	0.6
PM3-40-04	568	698	7	0.81	0.05022	0.00274	0.05136	0.00270	0.00742	0.00013	205	122	50.9	2.6	47.6	0.8
PM3-40-05	560	628	7	0.89	0.05124	0.00305	0.05026	0.00286	0.00711	0.00014	251	131	49.8	2.8	45.7	0.9
PM3-40-06	705	1096	10	0.64	0.05487	0.00269	0.05503	0.00258	0.00727	0.00013	407	106	54.4	2.5	46.7	0.8
PM3-40-07	1200	1403	14	0.86	0.04904	0.00206	0.04919	0.00198	0.00727	0.00011	150	96	48.8	1.9	46.7	0.7
PM3-40-08	584	904	8	0.65	0.04734	0.00220	0.04823	0.00216	0.00739	0.00011	66	108	47.8	2.1	47.5	0.7
PM3-40-09	453	795	8	0.57	0.04949	0.00311	0.04817	0.00291	0.00706	0.00014	171	141	47.8	2.8	45.3	0.9
PM3-40-10	1741	1088	13	1.60	0.05371	0.00289	0.05353	0.00276	0.00723	0.00013	359	116	52.9	2.7	46.4	0.8
PM3-40-11	1290	1906	18	0.68	0.04697	0.00156	0.04785	0.00153	0.00739	0.00010	48	78	47.5	1.5	47.5	0.6

Table S1 (Continued)

Sample spots	Th ppm	U ppm	Pb* ppm	Th/U	Ratios $^{207}Pb/^{206}Pb$	1σ	$^{207}Pb/^{235}U$	1σ	$^{206}Pb/^{238}U$	1σ	Age(Ma,1σ) $^{207}Pb/^{206}Pb$	1σ	$^{207}Pb/^{235}U$	1σ	$^{206}Pb/^{238}U$	1σ
PM3-40-12	647	1039	9	0.62	0.05346	0.00285	0.05330	0.00272	0.00723	0.00013	348	116	52.7	2.6	46.4	0.8
PM3-40-13	782	874	8	0.89	0.05485	0.00291	0.05553	0.00283	0.00734	0.00013	406	114	54.9	2.7	47.2	0.8
PM3-40-14	5592	2646	30	2.11	0.05083	0.00153	0.05034	0.00145	0.00718	0.00009	233	68	49.9	1.4	46.1	0.6
PM3-40-15	1247	1335	13	0.93	0.04733	0.00238	0.04678	0.00226	0.00717	0.00012	65	116	46.4	2.2	46	0.8
PM8-35 (29°51'42.9" 84°33'57.2")																
PM8-35-01	591	793	7	0.74	0.05204	0.00269	0.05396	0.00267	0.00752	0.00013	287	114	53.4	2.6	48.3	0.9
PM8-35-02	2676	1341	15	2.00	0.04775	0.00273	0.04867	0.00268	0.00739	0.00013	86	131	48.3	2.6	47.5	0.9
PM8-35-03	132	1232	9	0.11	0.05089	0.00200	0.05218	0.00197	0.00744	0.00011	236	88	51.6	1.9	47.8	0.7
PM8-35-04	234	522	5	0.45	0.04769	0.00356	0.04890	0.00351	0.00744	0.00017	83	169	48.5	3.4	47.8	1.1
PM8-35-05	308	309	3	1.00	0.05205	0.00541	0.05271	0.00535	0.00735	0.00018	288	221	52.2	5.2	47.2	1.2
PM8-35-06	1203	1495	17	0.80	0.04979	0.00294	0.05077	0.00287	0.00740	0.00014	185	132	50.3	2.8	47.5	0.9
PM8-35-07	431	767	7	0.56	0.05220	0.00347	0.05272	0.00336	0.00733	0.00016	294	145	52.2	3.2	47.1	1.0
PM8-35-08	575	812	8	0.71	0.04663	0.00288	0.04832	0.00289	0.00752	0.00014	30	142	47.9	2.8	48.3	0.9
PM8-35-09	508	957	8	0.53	0.04677	0.00239	0.04642	0.00229	0.00720	0.00012	37	118	46.1	2.2	46.3	0.8
PM8-35-10	1181	1158	11	1.02	0.05526	0.00232	0.05582	0.00224	0.00733	0.00011	423	91	55.1	2.2	47.1	0.7
PM8-35-11	464	686	6	0.68	0.05308	0.00296	0.05362	0.00286	0.00733	0.00014	332	122	53	2.8	47.1	0.9
PM8-35-12	922	1182	11	0.78	0.04962	0.00218	0.05053	0.00213	0.00739	0.00011	177	99	50.1	2.1	47.4	0.7
PM8-35-13	522	857	7	0.61	0.05043	0.00248	0.05026	0.00237	0.00723	0.00012	215	110	49.8	2.3	46.4	0.8
PM8-35-14	656	1010	9	0.65	0.04662	0.00219	0.04737	0.00214	0.00737	0.00012	30	109	47	2.1	47.3	0.8
PM8-35-15	734	1059	9	0.69	0.05173	0.00288	0.05277	0.00282	0.00740	0.00014	273	123	52.2	2.7	47.5	0.9
PM8-35-16	670	644	6	1.04	0.04783	0.00271	0.04847	0.00264	0.00735	0.00013	90	130	48.1	2.6	47.2	0.8

Table S1 (Continued)

Sample spots	Th ppm	U ppm	Pb* ppm	Th/U	Ratios $^{207}Pb/^{206}Pb$	1σ	$^{207}Pb/^{235}U$	1σ	$^{206}Pb/^{238}U$	1σ	Age(Ma,1σ) $^{207}Pb/^{206}Pb$	1σ	$^{207}Pb/^{235}U$	1σ	$^{206}Pb/^{238}U$	1σ
South																
PM12-11(29°49'14.4"	84°40'13.2")															
PM12-11-01	1046	789	8.2	1.33	0.04904	0.00269	0.05065	0.00268	0.00749	0.00013	150	124	50.2	2.6	48.1	0.9
PM12-11-02	1146	939	9.3	1.22	0.05079	0.00265	0.05141	0.00257	0.00734	0.00013	231	116	50.9	2.5	47.1	0.8
PM12-11-03	514	814	7.9	0.63	0.05280	0.00263	0.05628	0.00270	0.00773	0.00013	320	109	55.6	2.6	49.6	0.8
PM12-11-04	427	624	6.6	0.68	0.05165	0.00420	0.05348	0.00416	0.00751	0.00019	270	176	52.9	4.0	48.2	1.2
PM12-11-05	501	522	4.6	0.96	0.04262	0.00514	0.04352	0.00510	0.00740	0.00022	0	86	43.3	5.0	47.6	1.4
PM12-11-06	614	791	6.7	0.78	0.05004	0.00340	0.05217	0.00340	0.00756	0.00016	197	150	51.6	3.3	48.6	1.0
PM12-11-07	857	934	9.3	0.92	0.07889	0.00284	0.08215	0.00277	0.00755	0.00012	1170	70	80.2	2.6	48.5	0.8
PM12-11-08	593	510	5.1	1.16	0.06545	0.00401	0.06745	0.00392	0.00747	0.00016	789	124	66.3	3.7	48	1.1
PM12-11-09	828	964	9.3	0.86	0.05829	0.00291	0.05920	0.00282	0.00736	0.00013	540	106	58.4	2.7	47.3	0.9
PM12-11-10	908	1178	11.0	0.77	0.06502	0.00320	0.06666	0.00310	0.00743	0.00014	775	100	65.5	3.0	47.7	0.9
PM12-11-11	1104	3319	24.7	0.33	0.04877	0.00197	0.04949	0.00191	0.00736	0.00011	137	92	49	1.9	47.3	0.7
PM12-11-12	995	978	9.8	1.02	0.04898	0.00272	0.05055	0.00269	0.00749	0.00014	147	125	50.1	2.6	48.1	0.9
PM12-11-13	307	515	4.4	0.60	0.04641	0.00359	0.04862	0.00364	0.00760	0.00017	19	176	48.2	3.5	48.8	1.1
PM12-11-14	604	698	7.3	0.86	0.06964	0.00304	0.07297	0.00302	0.00760	0.00013	918	87	71.5	2.9	48.8	0.8
PM12-11-15	479	973	8.0	0.49	0.04865	0.00299	0.05043	0.00297	0.00752	0.00015	131	138	50	2.9	48.3	1.0
PM12-11-16	588	633	6.2	0.93	0.04963	0.00464	0.05077	0.00455	0.00742	0.00021	178	204	50.3	4.4	47.6	1.4
PM12-11-17	783	580	7.4	1.35	0.06573	0.00468	0.06747	0.00454	0.00744	0.00019	798	143	66.3	4.3	47.8	1.2

Table S1 (Continued)

Sample spots	Th ppm	U ppm	Pb* ppm	Th/U	f_{206}*(%)	Ratio $^{207}Pb/^{235}U$	±σ(%)	$^{206}Pb/^{238}U$	±σ(%)	$^{207}Pb/^{206}Pb$	±σ	Age(Ma,1σ) $^{207}Pb/^{235}U$	±σ	$^{206}Pb/^{238}U$	±σ
								SIMS							
North															
PM4-36 (29°56'6.2" 84°57'38.5")															
PM4-36@01	686.6	616.8	6.3	1.11	1.88	0.04567	6.93	0.00747	1.52120	-91.9	158.0	45.3	3.1	48.0	0.7
PM4-36@02	513.5	525.7	5.3	0.98	1.59	0.05183	9.90	0.00752	1.61613	193.0	212.5	51.3	5.0	48.3	0.8
PM4-36@03	276.6	313.4	3.0	0.88	9.02	0.05367	29.09	0.00748	1.84815	286.9	555.2	53.1	15.2	48.0	0.9
PM4-36@04	663.8	924.3	8.6	0.72	3.57	0.04471	8.48	0.00749	1.64242	-149.1	194.6	44.4	3.7	48.1	0.8
PM4-36@05	920.8	599.1	6.7	1.54	0.94	0.04941	4.54	0.00758	1.79685	62.0	96.4	49.0	2.2	48.7	0.9
PM4-36@06	863.5	1068.1	10.1	0.81	0.89	0.04966	6.79	0.00747	1.59094	108.1	149.0	49.2	3.3	48.0	0.8
PM4-36@07	617.3	987.5	8.8	0.63	1.15	0.04815	6.99	0.00731	1.66789	88.2	153.6	47.8	3.3	46.9	0.8
PM4-36@08	573.2	594.6	5.7	0.96	1.50	0.04436	11.38	0.00740	1.61701	-141.6	258.0	44.1	4.9	47.6	0.8
PM4-36@09	198.3	240.7	2.3	0.82	3.10	0.04536	21.11	0.00738	1.62401	-78.7	448.1	45.0	9.3	47.4	0.8
PM4-36@10	600.2	753.9	7.2	0.80	0.74	0.05092	4.92	0.00743	1.55831	180.1	105.4	50.4	2.4	47.7	0.7
PM8-35 (29°51'42.9" 84°33'57.2")															
PM8-35@01	195	1906	15	0.10		0.04628	1.89	0.0072	1.51	30.8	27.1	45.9	0.8	46.2	0.7
PM8-35@02	1735	1821	18	0.95	0.31	0.04600	1.93	0.0072	1.52	0.0	35.1	45.7	0.9	46.4	0.7
PM8-35@03	402	619	6	0.65	0.33	0.04841	2.84	0.0073	1.54	94.1	55.5	48.0	1.3	47.1	0.7
PM8-35@04	1316	1699	16	0.77		0.04758	2.27	0.0074	1.56	33.5	38.9	47.2	1.0	47.5	0.7
PM8-35@05	657	1970	17	0.33	0.32	0.04697	2.03	0.0074	1.54	-4.5	31.6	46.6	0.9	47.6	0.7
PM8-35@06	183	1107	9	0.16	0.00	0.04716	2.27	0.0075	1.50	-10.3	40.6	46.8	1.0	47.9	0.7
PM8-35@07	1313	2029	19	0.65	0.18	0.04812	1.93	0.0075	1.50	29.5	28.7	47.7	0.9	48.1	0.7
PM8-35@08	1010	1606	15	0.63	0.21	0.04856	2.09	0.0075	1.58	37.3	32.4	48.1	1.0	48.4	0.8
PM8-35@09	1145	2237	20	0.51	0.46	0.04851	1.91	0.0075	1.52	31.2	27.4	48.1	0.9	48.4	0.7
PM8-35@10	4102	2063	27	1.99	0.01	0.04928	1.94	0.0077	1.53	0.0	37.5	48.8	0.9	49.7	0.8
PM3-66 (29°56'48.9" 84°47'49.4")															
PM3-66@01	363	482	5	0.75	0.21	0.04655	4.90	0.0074	1.74	-14.3	107.1	46.2	2.2	47.4	0.8
PM3-66@02	828	567	6	1.46	0.36	0.04718	2.90	0.0074	1.50	0.0	58.8	46.8	1.3	47.7	0.7
PM3-66@04	761	661	7	1.15	0.17	0.04797	2.93	0.0075	1.55	22.0	58.6	47.6	1.4	48.1	0.7
PM3-66@06	635	611	6	1.04	0.30	0.04888	2.75	0.0076	1.71	38.8	50.7	48.5	1.3	48.7	0.8
PM3-66@07	426	509	5	0.84	0.20	0.04717	3.53	0.0076	1.54	-49.6	75.7	46.8	1.6	48.7	0.7
PM3-66@08	591	544	6	1.09	0.06	0.04706	3.30	0.0076	1.51	-55.8	55.8	46.7	1.5	48.7	0.7
PM3-66@09	607	643	7	0.94	0.02	0.04531	3.75	0.0076	1.50	-162.2	83.3	45.0	1.7	49.0	0.7
PM3-66@10	554	549	6	1.01	0.12	0.04804	3.23	0.0077	1.59	-31.3	66.7	47.6	1.5	49.2	0.8

Table S1 (Continued)

Sample spots	Th	U	Pb*	Th/U	f_{206}*(%)	Ratio				Age(Ma,1σ)					
	ppm	ppm	ppm			$^{207}Pb/^{235}U$	±σ(%)	$^{206}Pb/^{238}U$	±σ(%)	$^{207}Pb/^{206}Pb$	±σ	$^{207}Pb/^{235}U$	±σ	$^{206}Pb/^{238}U$	±σ
South															
PM12-11(29°49'14.4" 84°40'13.2")															
PM12-11@01	753.0	599.4	6.5	1.26	0.83	0.04973	6.56	0.00757	1.57089	81.1	144.5	49.3	3.2	48.6	0.8
PM12-11@02	464.2	553.9	5.2	0.84	1.24	0.04346	7.85	0.00734	1.67281	-170.9	170.9	43.2	3.3	47.1	0.8
PM12-11@03	196.3	447.2	3.8	0.44	1.73	0.04657	11.10	0.00737	1.55513	-10.7	246.2	46.2	5.0	47.3	0.7
PM12-11@04	575.0	1062.8	9.4	0.54	1.14	0.04358	7.24	0.00743	1.59997	-193.0	167.9	43.3	3.1	47.7	0.8
PM12-11@05	269.2	375.5	3.4	0.72	2.41	0.04733	12.88	0.00721	1.59173	80.5	278.3	47.0	5.9	46.3	0.7
PM12-11@06	319.4	332.7	3.3	0.96	1.55	0.04998	11.03	0.00746	1.56820	127.3	238.6	49.5	5.3	47.9	0.7
PM12-11@07	698.0	966.4	8.5	0.72	1.13	0.04265	6.48	0.00716	1.55464	-155.3	149.4	42.4	2.7	46.0	0.7
PM12-11@08	620.2	1351.5	11.1	0.46	0.80	0.04407	5.73	0.00713	1.50607	-64.0	129.7	43.8	2.5	45.8	0.7
PM12-11@09	758.5	535.0	5.8	1.42	1.05	0.04597	4.97	0.00753	1.80474	-96.5	96.5	45.6	2.2	48.4	0.9
PM12-11@10	1589.7	1589.2	15.7	1.00	0.32	0.04903	3.09	0.00741	1.51717	99.0	62.5	48.6	1.5	47.6	0.7
PM12-6(29°49'14.4" 84°40'13.2")															
PM12-06@01	715.2	818.6	8.3	0.87	0.00	0.05029	2.44	0.00763	1.56774	88.2	43.6	49.8	1.2	49.0	0.8
PM12-06@02	568.1	587.5	6.2	0.97	0.12	0.04999	2.53	0.00770	1.58580	53.9	46.3	49.5	1.2	49.4	0.8
PM12-06@03	129.9	166.1	1.6	0.78	0.01	0.05339	3.69	0.00751	2.04951	267.2	68.8	52.8	1.9	48.2	1.0
PM12-06@04	228.9	232.1	2.4	0.99	0.44	0.04714	4.28	0.00755	1.50010	-41.0	94.6	46.8	2.0	48.5	0.7
PM12-06@05	303.3	247.2	2.7	1.23	0.04	0.05080	4.39	0.00768	1.51386	97.6	94.6	50.3	2.2	49.3	0.7
PM12-06@06	532.1	528.9	5.5	1.01	0.15	0.04921	2.28	0.00767	1.50480	26.4	40.7	48.8	1.1	49.2	0.7
PM12-06@07	248.6	337.7	3.2	0.74	0.21	0.04814	3.37	0.00749	1.58285	30.1	69.9	47.7	1.6	48.1	0.8
PM12-06@08	647.2	963.5	9.4	0.67	0.02	0.05218	2.10	0.00775	1.50016	140.9	34.2	51.6	1.1	49.7	0.7
PM12-06@09	1836.8	1353.2	15.0	1.36	0.08	0.04827	2.00	0.00754	1.55372	18.8	30.1	47.9	0.9	48.5	0.8
PM12-06@10	650.9	634.6	6.5	1.03	0.08	0.04819	2.59	0.00748	1.54762	35.4	49.1	47.8	1.2	48.0	0.7
PM12-06@11	239.2	298.2	2.9	0.80	0.06	0.05168	2.90	0.00754	1.50469	182.0	56.8	51.2	1.4	48.4	0.7

Table S2 Major (wt%) and trace (ppm) element contents of the Lopu Range batholith

Sample	PM3-3	PM3-17	PM3-40	PM4-35	PM4-36	PM4-42	PM4-57	PM2-63	PM4-64
GPS	30°0'5.1"	29°59'21.8"	29°58'1.6"	29°56'6.9"	29°56'6.2"	29°56'2"	29°54'37.3"	29°54'11.4"	29°54'7.1"
	84°48'0.4"	84°47'51.9"	84°47'43.9"	84°57'44.1"	84°57'38.5"	84°57'17.1"	84°56'57.9"	84°57'23.9"	84°57'28.4"
					North				
Type	Monzogranite	Monzogranite	Granite	Granite	Monzogranite	Monzogranite	Monzogranite	Monzogranite	Granite
SiO_2	68.5	67.9	74.0	73.3	66.4	65.1	67.6	64.6	75.7
TiO_2	0.51	0.57	0.29	0.41	0.65	0.63	0.54	0.74	0.23
Al_2O_3	14.3	14.4	12.8	12.4	14.4	14.9	14.4	14.6	12.3
Fe_2O_3	1.54	1.50	0.82	0.96	1.84	2.12	1.24	1.87	0.79
FeO	1.87	2.40	1.30	0.98	1.97	2.20	2.25	3.10	0.65
MnO	0.06	0.06	0.03	0.04	0.07	0.08	0.09	0.10	0.03
MgO	1.57	1.68	0.67	1.12	1.98	2.23	1.87	2.29	0.60
CaO	2.79	2.34	1.54	1.90	3.36	4.24	2.69	3.19	1.21
Na_2O	3.19	3.16	2.85	2.83	3.05	3.12	3.23	2.89	2.91
K_2O	4.62	4.71	4.87	5.08	4.95	4.10	4.77	4.60	4.73
P_2O_5	0.16	0.19	0.08	0.17	0.24	0.23	0.21	0.24	0.09
LOI	0.52	0.62	0.52	0.55	0.64	0.57	0.71	1.11	0.54
Total	99.62	99.49	99.71	99.75	99.57	99.54	99.67	99.34	99.76
A/CNK	0.93	0.99	1.00	0.91	0.87	0.86	0.94	0.94	1.01
$Mg^{\#}$	46	44	37	52	49	49	49	46	44
K_2O/Na_2O	1.45	1.49	1.71	1.80	1.62	1.31	1.48	1.59	1.63
Sc	7.20	8.44	3.69	6.66	9.75	11.6	8.43	10.4	3.49
V	58.2	63.9	26.0	34.5	72.9	87.9	65.8	80.5	26.7
Cr	45.0	53.0	32.3	29.6	32.0	42.6	44.9	45.9	14.1
Co	11.9	16.4	12.1	17.1	18.7	23.3	18.5	15.3	22.1
Ni	21.0	24.4	11.7	12.2	19.1	21.5	23.0	26.7	8.08
Cu	17.7	14.2	14.2	7.95	5.80	15.2	6.60	7.58	4.84
Zn	50.4	61.5	39.9	35.7	53.3	60.8	54.4	63.9	37.5
Ga	17.8	19.5	16.0	17.8	19.1	19.1	19.4	18.8	16.3
Ge	2.16	2.45	1.79	2.02	2.33	2.37	2.29	2.65	1.50
Rb	347	413	349	389	351	221	460	329	478
Sr	415	373	271	144	434	479	443	441	147
Y	13.4	16.7	10.7	13.6	21.1	19.1	14.7	27.9	7.10
Zr	162	208	118	160	154	147	168	191	96.3
Nb	19.1	22.8	16.4	21.2	20.8	14.5	19.3	22.6	12.2
Cs	17.3	27.5	20.7	24.2	18.0	13.5	22.5	14.9	17.4
Ba	652	597	251	136	767	697	773	697	152
La	59.7	64.0	55.8	57.5	64.4	54.9	49.0	64.8	43.1
Ce	106	125	88.9	97.3	125	107	103	136	63.7
Pr	11.4	12.9	8.74	9.81	14.2	12.2	11.5	16.2	5.66

Nd	38.7	43.8	27.5	31.9	49.1	43.5	40.0	57.1	17.2
Sm	5.93	6.84	4.02	4.83	7.99	7.44	6.30	9.80	2.51
Eu	1.06	1.08	0.65	0.68	1.30	1.30	1.06	1.39	0.39
Gd	4.31	5.04	3.10	3.80	6.01	5.83	4.53	7.42	2.01
Tb	0.52	0.62	0.37	0.47	0.77	0.73	0.56	1.01	0.23
Dy	2.67	3.30	1.94	2.49	4.08	3.82	2.90	5.36	1.22
Ho	0.52	0.66	0.39	0.50	0.81	0.75	0.56	1.07	0.25
Er	1.43	1.81	1.13	1.43	2.16	2.01	1.52	2.93	0.75
Tm	0.22	0.28	0.18	0.23	0.34	0.30	0.23	0.45	0.13
Yb	1.49	1.92	1.30	1.64	2.22	2.00	1.60	2.96	0.93
Lu	0.25	0.30	0.22	0.29	0.34	0.31	0.25	0.46	0.16
Hf	5.53	6.76	4.54	6.15	4.90	4.64	5.32	5.97	4.39
Ta	2.23	2.68	2.35	2.38	2.58	1.21	2.01	2.61	1.88
Pb	41.6	36.0	46.8	32.5	34.2	33.4	32.9	33.3	33.3
Th	49.9	73.0	51.9	52.9	54.0	27.4	45.9	61.6	42.4
U	6.32	11.1	8.74	26.2	11.5	5.46	7.28	12.5	66.1
Sr/Y	30.9	22.4	25.3	10.6	20.5	25.1	30.2	15.8	20.7
Eu/Eu*	0.64	0.56	0.56	0.49	0.57	0.60	0.61	0.50	0.53
$(La/Yb)_N$	28.8	23.9	30.8	25.1	20.8	19.7	22.0	15.7	33.1
$(Ho/Yb)_N$	1.05	1.02	0.91	0.92	1.09	1.13	1.05	1.08	0.82
T_{Zr}	713	745	707	718	688	677	713	719	693

Table S2 (Continued)

Sample	PM4-68	PM4-69	PM8-4	PM8-7	PM8-9	PM8-31	PM8-34	PM8-35	PM4-5
	29°53'48.2"	29°53'40.7"	29°54'16.3"	29°54'4.9"	29°53'53.9"	29°52'2"	29°51'48.7"	29°51'42.9"	29°58'52.2"
GPS	84°57'38.4"	84°57'40.7"	84°32'21.5"	84°32'26.9"	84°32'31.2"	84°33'55.9"	84°33'57.9"	84°33'57.2"	84°59'25.4"
					North				
Type	Granite	Monzogranite	Granite	Granite	Granite	Granite	Granite	Monzogranite	Monzogranite
SiO_2	74.1	65.9	72.7	73.1	74.7	75.1	73.2	67.0	68.6
TiO_2	0.28	0.67	0.19	0.21	0.20	0.15	0.19	0.58	0.57
Al_2O_3	13.2	14.6	14.0	14.3	12.9	12.8	13.5	14.0	13.5
Fe_2O_3	0.78	1.85	0.73	0.76	0.90	0.58	0.70	2.20	1.74
FeO	0.80	2.05	1.40	1.35	1.30	0.93	1.53	2.40	1.75
MnO	0.04	0.07	0.04	0.05	0.05	0.02	0.03	0.08	0.08
MgO	0.78	2.05	0.42	0.26	0.24	0.22	0.40	1.77	1.84
CaO	1.49	3.73	1.30	0.89	0.89	0.93	1.36	3.10	3.11
Na_2O	2.60	2.98	3.62	3.29	3.02	3.53	3.35	3.04	3.17
K_2O	5.00	4.65	5.05	5.23	5.29	5.02	4.84	4.28	4.41
P_2O_5	0.10	0.25	0.11	0.04	0.04	0.04	0.09	0.18	0.23
LOI	0.58	0.67	0.09	0.08	0.08	0.45	0.27	0.93	0.63
Total	99.75	99.54	99.60	99.59	99.63	99.73	99.48	99.56	99.67
A/CNK	1.06	0.88	1.01	1.13	1.05	0.99	1.02	0.92	0.86
$Mg^{\#}$	48	49	26	18	17	21	25	42	49
K_2O/Na_2O	1.92	1.56	1.40	1.59	1.75	1.42	1.44	1.41	1.39
Sc	3.82	9.81	5.60	4.02	3.57	5.80	4.63	7.85	8.60
V	26.6	79.6	15.9	12.1	11.9	8.50	13.3	59.1	66.4
Cr	16.6	40.8	29.3	16.7	13.3	10.5	21.6	37.5	52.5
Co	20.3	19.7	13.0	14.2	15.0	11.6	12.4	13.8	14.5
Ni	8.37	20.7	8.52	5.22	5.42	2.98	4.43	24.2	25.9
Cu	7.43	13.6	9.34	5.51	4.65	7.51	6.63	6.61	9.16
Zn	44.7	122	32.9	29.4	36.3	14.9	35.7	39.9	69.6
Ga	15.6	19.2	16.7	16.9	16.8	19.3	18.6	17.9	18.6
Ge	1.52	2.51	1.79	1.78	1.78	1.76	1.75	2.12	2.39
Rb	449	332	450	484	420	712	396	419	414
Sr	221	434	111	69.1	84.8	63.6	142	423	379
Y	9.30	19.6	33.5	6.71	14.5	17.6	10.4	15.2	14.4
Zr	85.4	153	113	123	141	86.5	103	156	168
Nb	14.9	18.6	16.6	21.5	20.1	43.6	14.0	18.6	19.3
Cs	22.4	19.0	17.3	23.0	17.6	23.4	26.4	38.8	27.8
Ba	333	697	377	136	138	116	207	542	467
La	46.1	58.4	31.7	81.4	101	40.0	107	55.8	47.3
Ce	76.4	119	64.4	124	156	71.4	164	107	102

Pr	7.14	13.6	7.28	10.1	13.6	6.81	13.3	12.1	11.6
Nd	21.9	46.9	25.4	24.8	36.4	19.6	32.2	42.3	40.0
Sm	3.15	7.55	5.41	2.39	4.71	2.91	2.97	6.63	6.32
Eu	0.51	1.28	0.65	0.33	0.40	0.28	0.45	1.15	1.08
Gd	2.56	5.66	5.23	2.29	4.17	2.51	3.22	4.69	4.51
Tb	0.30	0.72	0.99	0.19	0.50	0.36	0.35	0.58	0.55
Dy	1.61	3.83	6.05	0.99	2.73	2.14	1.91	3.00	2.85
Ho	0.33	0.75	1.22	0.21	0.53	0.47	0.36	0.58	0.56
Er	0.98	2.04	3.31	0.72	1.49	1.50	0.97	1.57	1.49
Tm	0.17	0.31	0.49	0.15	0.24	0.28	0.15	0.24	0.23
Yb	1.19	2.04	3.03	1.33	1.61	2.23	0.99	1.57	1.56
Lu	0.21	0.32	0.46	0.27	0.25	0.40	0.16	0.25	0.25
Hf	3.41	4.81	3.99	4.74	5.03	4.23	3.83	4.94	5.39
Ta	1.83	2.03	2.55	3.41	3.11	8.06	1.69	2.05	2.07
Pb	38.0	55.6	67.3	58.4	55.0	40.1	59.4	35.4	32.3
Th	35.9	53.4	27.8	72.0	81.2	41.4	79.7	51.3	63.5
U	15.6	8.28	7.73	25.8	25.4	31.7	10.7	12.4	7.91
Sr/Y	23.8	22.1	3.32	10.3	5.83	3.60	13.6	27.8	26.3
Eu/Eu*	0.55	0.60	0.37	0.43	0.28	0.32	0.44	0.63	0.62
$(La/Yb)_N$	27.7	20.5	7.50	43.7	45.0	12.9	77.6	25.4	21.7
$(Ho/Yb)_N$	0.83	1.10	1.21	0.48	1.00	0.63	1.10	1.11	1.07
T_{Zr}	686	687	700	726	733	677	695	702	700

Table S2 (Continued)

Sample	PM3-66	PM12-6	PM12-11
	29°56'48.9"	29°49'14.4"	29°49'14.4"
GPS	84°47'49.4"	84°40'13.2"	84°40'13.2"
	North	**South**	
Type	Monzogranite	Monzogranite	Monzogranite
SiO_2	64.4	64.9	64.3
TiO_2	0.67	0.68	0.73
Al_2O_3	14.9	14.9	15.1
Fe_2O_3	2.52	1.06	1.05
FeO	2.40	3.73	3.48
MnO	0.08	0.08	0.07
MgO	2.21	2.00	2.16
CaO	3.67	3.65	3.94
Na_2O	3.13	2.99	3.09
K_2O	4.46	4.59	4.54
P_2O_5	0.22	0.22	0.25
LOI	0.81	0.61	0.47
Total	99.49	99.40	99.18
A/CNK	0.90	0.90	0.88
$Mg^{\#}$	45	43	46
K_2O/Na_2O	1.42	1.54	1.47
Sc	10.8	10.0	10.5
V	83.0	77.8	83.6
Cr	44.4	36.6	39.2
Co	17.7	17.3	17.4
Ni	23.3	22.5	24.3
Cu	21.6	11.1	17.7
Zn	87.2	65.3	65.4
Ga	18.7	20.4	19.7
Ge	2.45	2.42	2.49
Rb	241	323	299
Sr	450	494	505
Y	20.9	19.6	19.3
Zr	174	182	217
Nb	14.9	18.6	19.2
Cs	10.2	44.8	57.7
Ba	737	711	768
La	54.2	63.5	61.5
Ce	108	126	122

Pr	12.3	14.3	14.0
Nd	43.6	49.6	49.6
Sm	7.38	8.17	7.94
Eu	1.28	1.36	1.36
Gd	5.74	5.69	5.83
Tb	0.77	0.72	0.72
Dy	4.15	3.86	3.76
Ho	0.83	0.73	0.74
Er	2.23	1.97	2.00
Tm	0.34	0.30	0.30
Yb	2.22	1.94	1.96
Lu	0.35	0.29	0.30
Hf	5.40	5.41	6.50
Ta	1.69	2.24	2.21
Pb	33.2	36.6	38.6
Th	35.9	51.4	47.9
U	2.89	6.86	7.72
Sr/Y	21.6	25.2	26.2
Eu/Eu*	0.60	0.61	0.61
$(La/Yb)_N$	17.5	23.5	22.5
$(Ho/Yb)_N$	1.12	1.12	1.13
T_{Zr}	699	706	715

$Mg^{\#} = Mg^{2+}\times100/(Mg^{2+} + Fe^{2+})$; A/CNK = $Al_2O_3/(CaO+Na_2O+K_2O)$molar; Eu/Eu* = $Eu_N/(Sm_N\times Gd_N)^{\wedge(1/2)}$,$Eu_N$, Sm_N and Gd_N, T_{Zr} were calculated by Boehnke et al., 2013 Chemical Geology (Boehnke, P., Watson, E.B., Trail, D., Harrison, T.M., Schmitt, A.K., 2013, Zircon saturation re-revisited. Chemical Geology, v. 351, p.324-334.)

Text S2 References cited in Data 1 and 3

REFERENCES CITED in Data 1

Bouilhol, P., Schaltegger, U., Chiaradia, M., Ovtcharova, M., Stracke, A., Burg, J.-P., and Dawood, H., 2011, Timing of juvenile arc crust formation and evolution in the Sapat Complex (Kohistan–Pakistan): Chemical Geology, v. 280, p. 243–256, https://doi.org/10.1016/j.chemgeo.2010.11.013.

Chen, L., Qin, K.Z., Li, G.M., Li, J.X., Xiao, B., Zhao, J.X., and Fan, X., 2015, Zircon U-Pb ages, geochemistry, and Sr-Nd-Pb-Hf isotopes of the Nuri intrusive rocks in the Gangdese area, southern Tibet: Constraints on timing, petrogenesis, and tectonic transformation: Lithos, v. 212, p. 379–396, https://doi.org/10.1016/j.lithos.2014.11.014.

Chu, M.F., Chung, S.L., O'Reilly, S.Y., Pearson, N.J., Wu, F.Y., Li, X.H., Liu, D.Y., Ji, J.Q., Chu, C.H., and Lee, H.Y., 2011, India's hidden inputs to Tibetan orogeny revealed by Hf isotopes of Transhimalayan zircons and host rocks: Earth and Planetary Science Letters, v. 307, p. 479–486, https://doi.org/10.1016/j.epsl.2011.05.020.

Chu, M.F., Chung, S.L., Song, B.A., Liu, D.Y., O'Reilly, S.Y., Pearson, N.J., Ji, J.Q., and Wen, D.J., 2006, Zircon U-Pb and Hf isotope constraints on the Mesozoic tectonics and crustal evolution of southern Tibet: Geology, v. 34, p. 745–748, https://doi.org/10.1130/G22725.1.

Guan, Q., Zhu, D.-C., Zhao, Z.-D., Dong, G.-C., Zhang, L.-L., Li, X.-W., Liu, M., Mo, X.-X., Liu, Y.-S., and Yuan, H.-L., 2012, Crustal thickening prior to 38 Ma in southern Tibet: Evidence from lower crust-derived adakitic magmatism in the Gangdese Batholith: Gondwana Research, v. 21, p. 88–99, https://doi.org/10.1016/j.gr.2011.07.004.

Guan, Q., Zhu, D.C., Zhao, Z.D., Dong, G.C., Mo, X.X., Liu, Y.S., Hu, Z.C., and Yuan, H.L., 2011, Zircon U-Pb chronology, geochemistry of the Late Cretaceous mafic magmatism in the southern Lhasa Terrane and its implications: Yanshi Xuebao, v. 27, p. 2083–2094.

Guan, Q., Zhu, D.C., Zhao, Z.D., Zhang, L.L., Liu, M., Li, X.W., Yu, F., and Mo, X.X., 2010, Late Cretaceous adakites in the eastern segment of the Gangdese Belt, southern Tibet: Products of Neo-Tethyan ridge subduction?: Yanshi Xuebao, v. 26, p. 2165–2179.

Guo, L., Zhang, H. F., Harris, N., Pan, F. B., and Xu, W. C., 2011, Origin and evolution of multi-stage felsic melts in eastern Gangdese belt: Constraints from U-Pb zircon dating and Hf isotopic composition. Lithos, v, 127, p. 54–67.

Heuberger, S., Schaltegger, U., Burg, J.-P., Villa, I.M., Frank, M., Dawood, H., Hussain, S., and Zanchi, A., 2007, Age and isotopic constraints on magmatism along the Karakoram-Kohistan Suture Zone, NW Pakistan: evidence for subduction and continued convergence after India-Asia collision: Swiss Journal of Geosciences, v. 100, p. 85–107, https://doi.org/10.1007/s00015-007-1203-7.

Ji, W.Q., Wu, F.Y., Chung, S.L., Li, J.X., and Liu, C.Z., 2009, Zircon U-Pb geochronology and Hf isotopic constraints on petrogenesis of the Gangdese batholith, southern Tibet: Chemical Geology, v. 262, p. 229–245, https://doi.org/10.1016/j.chemgeo.2009.01.020.

Ji, W.Q., Wu, F.Y., Chung, S.L., and Liu, C.Z., 2014, The Gangdese magmatic constraints on a latest Cretaceous lithospheric delamination of the Lhasa terrane, southern Tibet: Lithos, v. 210, p. 168–180, https://doi.org/10.1016/j.lithos.2014.10.001.

Ji, W.Q., Wu, F.Y., Liu, C.Z., and Chung, S.L., 2012, Early Eocene crustal thickening in southern Tibet: New age and geochemical constraints from the Gangdese batholith: Journal of Asian Earth Sciences, v. 53, p. 82–95, https://doi.org/10.1016/j.jseaes.2011.08.020.

Jia, L.L., 2014, Regional variation of geochemical characteristics and tectonic implication of the Early Eocene basic rocks in southern Tibet: Master thesis, China University of Geoscience (Beijing), p. 1–60.

Jiang, Z.Q., Wang, Q., Li, Z.X., Wyman, D.A., Tang, G.J., Jia, X.H., and Yang, Y.H., 2012, Late Cretaceous (ca. 90 Ma) adakitic intrusive rocks in the Kelu area, Gangdese Belt (southern Tibet): Slab melting and implications for Cu-Au mineralization: Journal of Asian Earth Sciences, v. 53, p. 67–81, https://doi.org/10.1016/j.jseaes.2012.02.010.

Jiang, Z.Q., Wang, Q., Wyman, D.A., Li, Z.X., Yang, J.H., Shi, X.B., Ma, L., Tang, G.J., Gou, G.N., Jia, X.H., and Guo, H.F., 2014, Transition from oceanic to continental lithosphere subduction in southern Tibet: Evidence from the Late Cretaceous-Early Oligocene (similar to 91–30 Ma) intrusive rocks in the Chanang-Zedong area, southern Gangdese: Lithos, v. 196, p. 213–231, https://doi.org/10.1016/j.lithos.2014.03.001.

Liu, A., Zhu, D., Wang, Q., Zhang, L., Li, S., Zhang, L., and Zhao, Z., 2015, LA-ICP-MS zircon U-Pb age and origin of the Linzizong volcanic rocks from Milashan, southern Tibet: Geological Bulletin of China, v. 34, p. 826–833.

Liu, Z.-C., Ding, L., Zhang, L.-Y., Wang, C., Qiu, Z.-L., Wang, J.-G., Shen, X.-L., and Deng, X.-Q., 2018, Sequence and petrogenesis of the Jurassic volcanic rocks (Yeba Formation) in the Gangdese arc, southern Tibet: Implications for the Neo-Tethyan subduction: Lithos, v. 312–313, p. 72–88, https://doi.org/10.1016/j.lithos.2018.04.026.

Liu, F., 2012, Cenozoic multistage adakitic magmatism and tectonic significance of the southeastern segment of the Gangdese belt, Tibetan Plateau: Master thesis, China University of Geosciences (Wuhan), p. 1–57.

Liu, Z.C., Wu, F.Y., Ji, W.Q., Wang, J.G., and Liu, C.Z., 2014, Petrogenesis of the Ramba leucogranite in the Tethyan Himalaya and constraints on the channel flow model: Lithos, v. 208, p. 118–136, https://doi.org/10.1016/j.lithos.2014.08.022.

Ma, L., Wang, B.D., Jiang, Z.Q., Wang, Q., Li, Z.X., Wyman, D.A., Zhao, S.R., Yang, J.H., Gou, G.N., and Guo, H.F., 2014, Petrogenesis of the Early Eocene adakitic rocks in the Napuri area, southern Lhasa: Partial melting of thickened lower crust during slab break-off and implications for crustal thickening in southern Tibet: Lithos, v. 196, p. 321–338, https://doi.org/10.1016/j.lithos.2014.02.011.

Ma, L., Wang, Q., Li, Z.X., Wyman, D.A., Jiang, Z.Q., Yang, J.H., Gou, G.N., and Guo, H.F., 2013a, Early Late Cretaceous (ca. 93 Ma) norites and hornblendites in the Milin area, eastern Gangdese: Lithosphere-asthenosphere interaction during slab roll-back and an insight into early Late Cretaceous (ca. 100–80 Ma) magmatic "flare-up" in southern Lhasa (Tibet): Lithos, v. 172, p. 17–30, https://doi.org/10.1016/j.lithos.2013.03.007.

Ma, L., Wang, Q., Wyman, D.A., Jiang, Z.Q., Yang, J.H., Li, Q.L., Gou, G.N., and Guo, H.F., 2013b, Late Cretaceous crustal growth in the Gangdese area, southern Tibet: Petrological and Sr-Nd-Hf-O isotopic evidence from Zhengga diorite-gabbro: Chemical Geology, v. 349, p. 54–70, https://doi.org/10.1016/j.chemgeo.2013.04.005.

Ma, L., Wang, Q., Wyman, D.A., Li, Z.X., Jiang, Z.Q., Yang, J.H., Gou, G.N., and Guo, H.F., 2013c, Late Cretaceous (100–89 Ma) magnesian charnockites with adakitic affinities in the Milin area, eastern Gangdese: Partial melting of subducted oceanic crust and implications for crustal growth in southern Tibet: Lithos, v. 175, p. 315–332, https://doi.org/10.1016/j.lithos.2013.04.006.

Ravikant, V., Wu, F.Y., and Ji, W.Q., 2009, Zircon U-Pb and Hf isotopic constraints on petrogenesis of the Cretaceous-Tertiary granites in eastern Karakoram and Ladakh, India: Lithos, v. 110, p. 153–166, https://doi.org/10.1016/j.lithos.2008.12.013.

Ran, M.-l., Kang, Z.-q., Xu, J.-f., Yang, F., Jiang, Z.-q., Li, Q., Wei, N.-s., Wei, T.-w., and Liu, D., 2019, Evolution of the northward subduction of the Neo-Tethys: Implications of geochemistry of Cretaceous arc volcanics in Qinghai-Tibetan Plateau: Palaeogeography, Palaeoclimatology, Palaeoecology, v. 515, p. 83–94, https://doi.org/10.1016/j.palaeo.2017.12.043.

Schaltegger, U., Zeilinger, G., Frank, M., and Burg, J.-P., 2002, Multiple mantle sources during island arc magmatism: U–Pb and Hf isotopic evidence from the Kohistan arc complex, Pakistan: Terra Nova, v. 14, p. 461–468, https://doi.org/10.1046/j.1365-3121.2002.00432.x.

Wang, R., Richards, J.P., Hou, Z.Q., An, F., and Creaser, R.A., 2015, Zircon U-Pb age and Sr-Nd-Hf-O isotope geochemistry of the Paleocene-Eocene igneous rocks in western Gangdese: Evidence for the timing of Neo-Tethyan slab breakoff: Lithos, v. 224, p. 179–194, https://doi.org/10.1016/j.lithos.2015.03.003.

Wu, F. Y., Ji, W. Q., Liu, C. Z., and Chung, S. L., 2010, Detrital zircon U-Pb and Hf isotopic data from the Xigaze fore-arc basin: Constraints on Transhimalayan magmatic evolution in southern Tibet. Chemical Geology, v, 271, p. 13–25.

Xu, W.C., 2010, Spatial variation of zircon U-Pb ages and Hf isotopic compositions of the Gangdese granitoids and its geologic implications: Ph.D thesis, China University of Geosciences (Wuhan), p. 1–172.

Zhang, Z.M., Dong, X., Xiang, H., Liou, J.G., and Santosh, M., 2013, Building of the Deep Gangdese Arc, South Tibet: Paleocene Plutonism and Granulite-Facies Metamorphism: Journal of Petrology, v. 54, p. 2547–2580, https://doi.org/10.1093/petrology/egt056.

Zheng, Y.C., Hou, Z.Q., Gong, Y.L., Liang, W., Sun, Q.Z., Zhang, S., Fu, Q., Huang, K.X., Li, Q.Y., and Li, W., 2014, Petrogenesis of Cretaceous adakite-like intrusions of the Gangdese Plutonic Belt, southern Tibet: Implications for mid-ocean ridge subduction and crustal growth: Lithos, v. 190, p. 240–263, https://doi.org/10.1016/j.lithos.2013.12.013.

Zhou, L.M., Wang, R., Hou, Z.-q., Li, C., Zhao, H., Li, X.-W., and Qu, W.-J., 2018, Hot Paleocene-Eocene Gangdese arc: Growth of continental crust in southern Tibet: Gondwana Research, v. 62, p. 178–197, https://doi.org/10.1016/j.gr.2017.12.011.

Zhu, D.C., Zhao, Z.D., Niu, Y.L., Mo, X.X., Chung, S.L., Hou, Z.Q., Wang, L.Q., and Wu, F.Y., 2011, The Lhasa Terrane: Record of a microcontinent and its histories of drift and growth: Earth and Planetary Science Letters, v. 301, p. 241–255, https://doi.org/10.1016/j.epsl.2010.11.005.

REFERENCES CITED in Data 3

Chen, L., Qin, K.Z., Li, G.M., Li, J.X., Xiao, B., Zhao, J.X., and Fan, X., 2015, Zircon U-Pb ages, geochemistry, and Sr-Nd-Pb-Hf isotopes of the Nuri intrusive rocks in the Gangdese area, southern Tibet: Constraints on timing, petrogenesis, and tectonic transformation: Lithos, v. 212, p. 379–396, https://doi.org/10.1016/j.lithos.2014.11.014.

Dong, G., Mo, X., Hao, Z., Zhu, D., Song, Y., and Wang, L., 2008, Gabbros from southern Gangdese: Implication for mass exchange between mantle and crust: Yanshi Xuebao, v. 24, p. 203–210.

Gao, Y.F., Wei, R.H., Hou, Z.Q., Tian, S.H., and Zhao, R.S., 2008, Eocene high-MgO volcanism in southern Tibet: New constraints for mantle source characteristics and deep processes: Lithos, v. 105, p. 63–72, https://doi.org/10.1016/j.lithos.2008.02.008.

Hou, Z.Q., Zheng, Y.C., Zeng, L.S., Gao, L.E., Huang, K.X., Li, W., Li, Q.Y., Fu, Q., Liang, W., and Sun, Q.Z., 2012, Eocene-Oligocene granitoids in southern Tibet: Constraints on crustal anatexis and tectonic evolution of the Himalayan orogeny: Earth and Planetary Science Letters, v. 349, p. 38–52, https://doi.org/10.1016/j.epsl.2012.06.030.

Huang, Y., Zhao, Z.D., Zhang, F.Q., Zhu, D.C., Dung, G.C., Zhou, S., and Mo, X.X., 2010, Geochemistry and implication of the Gangdese batholiths from Renbu and Lhasa areas in southern Gangdese, Tibet: Yanshi Xuebao, v. 26, p. 3131–3142.

Jiang, Z.Q., Wang, Q., Li, Z.X., Wyman, D.A., Tang, G.J., Jia, X.H., and Yang, Y.H., 2012, Late Cretaceous (ca. 90 Ma) adakitic intrusive rocks in the Kelu area, Gangdese Belt (southern Tibet): Slab melting and implications for Cu-Au mineralization: Journal of Asian Earth Sciences, v. 53, p. 67–81, https://doi.org/10.1016/j.jseaes.2012.02.010.

Jiang, Z.Q., Wang, Q., Wyman, D.A., Li, Z.X., Yang, J.H., Shi, X.B., Ma, L., Tang, G.J., Gou, G.N., Jia, X.H., and Guo, H.F., 2014, Transition from oceanic to continental lithosphere subduction in southern Tibet: Evidence from the Late Cretaceous-Early Oligocene (similar to 91–30 Ma) intrusive rocks in the Chanang-Zedong area, southern Gangdese: Lithos, v. 196, p. 213–231, https://doi.org/10.1016/j.lithos.2014.03.001.

Xie, K.J., Zeng, L.S., Liu, J., Gao, L.E., and Hue, G.Y., 2011, Timing and geochemistry of the Linzizong Group volcanic rocks in Sangsang area, Ngamring County, southern Tibet: Geological Bulletin of China, v. 30, p. 1339–1352.

Lee, H.Y., Chung, S.L., Ji, J., Qian, Q., Gallet, S., Lo, C.H., Lee, T.Y., and Zhang, Q., 2012, Geochemical and Sr-Nd isotopic constraints on the genesis of the Cenozoic Linzizong volcanic successions, southern Tibet: Journal of Asian Earth Sciences, v. 53, p. 96–114, https://doi.org/10.1016/j.jseaes.2011.08.019.

Liu, Z.C., Wu, F.Y., Ji, W.Q., Wang, J.G., and Liu, C.Z., 2014, Petrogenesis of the Ramba leucogranite in the Tethyan Himalaya and constraints on the channel flow model: Lithos, v. 208, p. 118–136, https://doi.org/10.1016/j.lithos.2014.08.022.

Liu, Z.-C., Ding, L., Zhang, L.-Y., Wang, C., Qiu, Z.-L., Wang, J.-G., Shen, X.-L., and Deng, X.-Q., 2018, Sequence and petrogenesis of the Jurassic volcanic rocks (Yeba Formation) in the Gangdese arc, southern Tibet: Implications for the Neo-Tethyan subduction: Lithos, v. 312–313, p. 72–88, https://doi.org/10.1016/j.lithos.2018.04.026.

Ma, L., Wang, B.D., Jiang, Z.Q., Wang, Q., Li, Z.X., Wyman, D.A., Zhao, S.R., Yang, J.H., Gou, G.N., and Guo, H.F., 2014, Petrogenesis of the Early Eocene adakitic rocks in the Napuri area, southern Lhasa: Partial melting of thickened lower crust during slab break-off and implications for crustal thickening in southern Tibet: Lithos, v. 196, p. 321–338, https://doi.org/10.1016/j.lithos.2014.02.011.

Ma, L., Wang, Q., Li, Z.X., Wyman, D.A., Jiang, Z.Q., Yang, J.H., Gou, G.N., and Guo, H.F., 2013a, Early Late Cretaceous (ca. 93 Ma) norites and hornblendites in the Milin area, eastern Gangdese: Lithosphere-asthenosphere interaction during slab roll-back and an insight into early Late Cretaceous (ca. 100–80 Ma) magmatic "flare-up" in southern Lhasa (Tibet): Lithos, v. 172, p. 17–30, https://doi.org/10.1016/j.lithos.2013.03.007.

Ma, L., Wang, Q., Wyman, D.A., Jiang, Z.Q., Yang, J.H., Li, Q.L., Gou, G.N., and Guo, H.F., 2013b, Late Cretaceous crustal growth in the Gangdese area, southern Tibet: Petrological and Sr-Nd-Hf-O isotopic evidence from Zhengga diorite-gabbro: Chemical Geology, v. 349, p. 54–70, https://doi.org/10.1016/j.chemgeo.2013.04.005.

Ma, L., Wang, Q., Wyman, D.A., Li, Z.X., Jiang, Z.Q., Yang, J.H., Gou, G.N., and Guo, H.F., 2013c, Late Cretaceous (100–89 Ma) magnesian charnockites with adakitic affinities in the Milin area, eastern Gangdese: Partial melting of subducted oceanic crust and implications for crustal growth in southern Tibet: Lithos, v. 175, p. 315–332, https://doi.org/10.1016/j.lithos.2013.04.006.

Mo, X., Niu, Y., Dong, G., Zhao, Z., Hou, Z., Zhou, S., and Ke, S., 2008, Contribution of syncollisional felsic magmatism to continental crust growth: A case study of the Paleogene Linzizong volcanic Succession in southern Tibet: Chemical Geology, v. 250, p. 49–67, https://doi.org/10.1016/j.chemgeo.2008.02.003.

Mo, X.X., Hou, Z.Q., Niu, Y.L., Dong, G.C., Qu, X.M., Zhao, Z.D., and Yang, Z.M., 2007, Mantle contributions to crustal thickening during continental collision: Evidence from Cenozoic igneous rocks in southern Tibet: Lithos, v. 96, p. 225–242, https://doi.org/10.1016/j.lithos.2006.10.005.

Ran, M.-l., Kang, Z.-q., Xu, J.-f., Yang, F., Jiang, Z.-Q., Li, Q., Wei, N.-S., Wei, T.-W., and Liu, D., 2018, Evolution of the northward subduction of the Neo-Tethys: Implications of geochemistry of Cretaceous arc volcanics in Qinghai-Tibetan Plateau: Palaeogeography, Palaeoclimatology, Palaeoecology, v. 515, p. 83–94, https://doi.org/10.1016/j.palaeo.2017.12.043.

Wang, R., Richards, J.P., Hou, Z.Q., An, F., and Creaser, R.A., 2015a, Zircon U-Pb age and Sr-Nd-Hf-O isotope geochemistry of the Paleocene-Eocene igneous rocks in western

Gangdese: Evidence for the timing of Neo-Tethyan slab breakoff: Lithos, v. 224, p. 179–194, https://doi.org/10.1016/j.lithos.2015.03.003.
Wang, R., Richards, J.P., Zhou, L.-m., Hou, Z.-q., Stern, R.A., Creaser, R.A., and Zhu, J.-J., 2015b, The role of Indian and Tibetan lithosphere in spatial distribution of Cenozoic magmatism and porphyry Cu–Mo deposits in the Gangdese belt, southern Tibet: Earth-Science Reviews, v. 150, p. 68–94, https://doi.org/10.1016/j.earscirev.2015.07.003.
Wen, D.R., Chung, S.L., Song, B., Iizuka, Y., Yang, H.J., Ji, J.Q., Liu, D.Y., and Gallet, S., 2008, Late Cretaceous Gangdese intrusions of adakitic geochemical characteristics, SE Tibet: Petrogenesis and tectonic implications: Lithos, v. 105, p. 1–11, https://doi.org/10.1016/j.lithos.2008.02.005.
Yang, Z.M., Hou, Z.Q., Jiang, Y.F., Zhang, H.R., and Song, Y.C., 2011, Sr-Nd-Pb and zircon Hf isotopic constraints on petrogenesis of the Late Jurassic granitic porphyry at Qulong, Tibet: Yanshi Xuebao, v. 27, p. 2003–2010.
Zeng, L.S., Gao, L.E., Xie, K.J., and Jing, L.Z., 2011, Mid-Eocene high Sr/Y granites in the Northern Himalayan Gneiss Domes: Melting thickened lower continental crust: Earth and Planetary Science Letters, v. 303, p. 251–266, https://doi.org/10.1016/j.epsl.2011.01.005.
Zheng, Y.C., Hou, Z.Q., Gong, Y.L., Liang, W., Sun, Q.Z., Zhang, S., Fu, Q., Huang, K.X., Li, Q.Y., and Li, W., 2014, Petrogenesis of Cretaceous adakite-like intrusions of the Gangdese Plutonic Belt, southern Tibet: Implications for mid-ocean ridge subduction and crustal growth: Lithos, v. 190, p. 240–263, https://doi.org/10.1016/j.lithos.2013.12.013.